

## Drift wave vs. interchange turbulence: geometrical effects on the ballooning threshold.

T.T. Ribeiro<sup>1,2</sup> and B. Scott<sup>1</sup>

<sup>1</sup> Max-Planck-Institut für Plasmaphysik, EURATOM Association, Garching, Germany

<sup>2</sup> Instituto de Plasmas e Fusão Nuclear, EURATOM/IST Association, Lisboa, Portugal

**Introduction:** The competition between drift wave and interchange physics plays a central role in the tokamak edge turbulence dynamics. They provide the mechanisms by which the thermal free energy is transferred from the background thermal gradient to the turbulent fluctuations. Whichever one dominates, for a given set a plasma parameters, will impose its character on the turbulence. At moderate plasma  $\beta$  and drift wave collisionality, the drift wave character prevails due to the effectiveness of the nonlinear vorticity advection, through which the self-sustained drift wave turbulence is able to scatter the structure of the linear instabilities apart before they can grow to become important [1]. As the collisionality is raised, the turbulence evolves into larger ballooning structures, for which the vorticity scattering is less effective, leaving room for the interchange effects to take over, and a gradual transition into resistive ballooning dynamics occurs. We assess the impact of the proximity to an X-point on this threshold, by means of turbulence computations, using both an S- $\alpha$  geometry and a simplified X-point geometry [2].

**Model:** The electromagnetic gyrofluid GEM [3] in its isothermal variation was used. The corresponding local (no zonal profile evolution) equations are, in gyro-Bohm normalised units [3]

$$\begin{aligned} \frac{\partial \tilde{n}_z}{\partial t} &= -\omega_n \frac{\partial \tilde{\phi}_z}{\partial y} - [\tilde{\phi}_z, \tilde{n}_z] - B \frac{\partial}{\partial s} \frac{\tilde{v}_{z\parallel}}{B} + \hat{\beta} [\tilde{A}_{\parallel}, \tilde{v}_{z\parallel}] + K(\tilde{\phi}_z + \tau_z \tilde{n}_z) \\ \hat{\beta} \frac{\partial \tilde{A}_{\parallel}}{\partial t} - \hat{\mu}_z \frac{\partial \tilde{v}_{z\parallel}}{\partial t} - \hat{\mu}_z [\tilde{\phi}_z, \tilde{v}_{z\parallel}] & \\ &= -B \frac{\partial}{\partial s} \frac{\tilde{\phi}_z + \tau_z \tilde{n}_z}{B} + \hat{\beta} [\tilde{A}_{\parallel}, \tilde{\phi}_z + \tau_z \tilde{n}_z] + \tau_z \hat{\beta} \omega_n \frac{\partial \tilde{A}_{\parallel}}{\partial y} + \hat{\mu}_z K(2\tilde{v}_{z\parallel}) - C\tilde{J}_{\parallel} \end{aligned} \quad (1)$$

for the the guiding centre density and parallel velocity for each species  $z$ , connected through the equations governing the induction (Ampère's law) and the polarisation

$$-\nabla_{\perp}^2 \tilde{A}_{\parallel} = \tilde{J}_{\parallel} = \tilde{u}_{\parallel} - \tilde{v}_{\parallel} \quad \Gamma_0^{1/2} \tilde{n}_i + \frac{\Gamma_0 - 1}{\tau_i} \tilde{\phi} = \tilde{n}_e \quad (2)$$

(for singly charged plasmas) in which  $\Gamma_0(b) = I_0(b)e^{-b}$  and  $I_0 = J_0(ib)$  is a modified Bessel function. The state variables are the electrostatic potentials ( $\tilde{\phi}_z = \Gamma_0^{1/2} \tilde{\phi}$ ) and densities ( $\tilde{n}_z$ ) and the flux variables are the particle parallel velocities ( $\tilde{v}_{z\parallel}$ ), where  $\tau_z = T_z/(ZT_e)$  and  $\mu_z = M_z/(ZM_i)$  ( $Z$  – charge number). The nonlinearities are represented by the square brackets which correspond to Poisson brackets in this field aligned formulation, where  $\{x, y, s\}$  are the radial, toroidal and poloidal directions, respectively. The curvature operator represents the only toroidal

effect of the S- $\alpha$  geometry and is expressed by  $K = \omega_B(\sin s \partial_x + \cos s \partial_y)$  for shifted metric [4]. The cold-ions limit  $T_i \rightarrow 0$  is invoked within this work for the sake of simplicity to make the X-point effects more transparent. In practice this makes for  $\Gamma_0 \rightarrow 1$  and  $(\Gamma_0 - 1)/\tau_i \rightarrow \nabla_{\perp}^2/B^2$ .

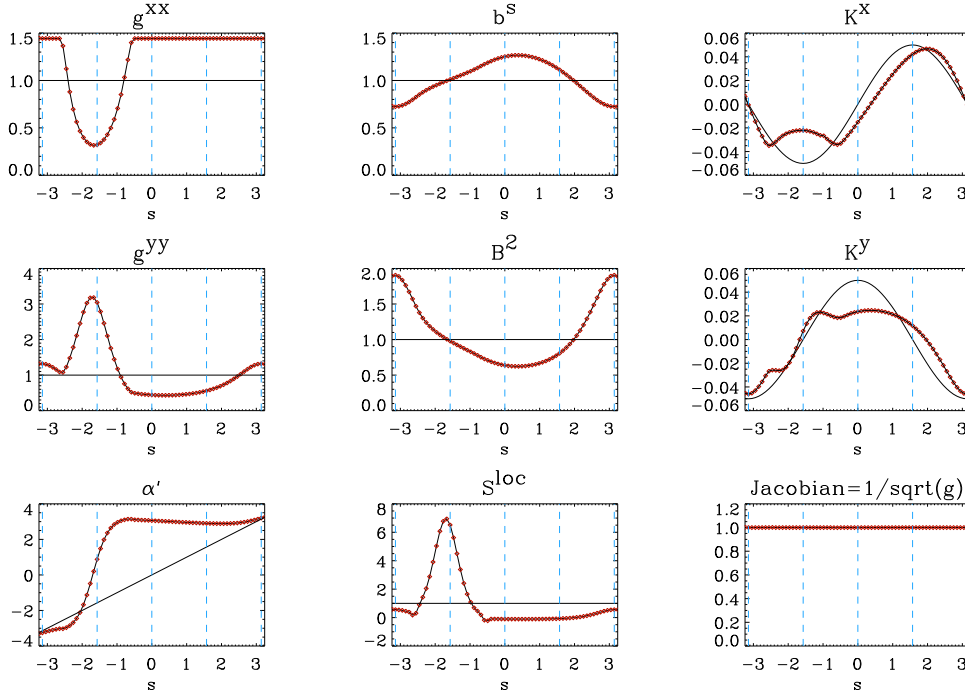


Figure 1: Geometrical quantities needed for the flux tube turbulence model. Both S- $\alpha$  (thin line) and X-point (dotted line) cases shown. Only  $s$ -coordinate dependence is kept. The X-point is at  $s \approx -\pi/2$ , where the local shear shows a distinct peak, and the outboard side at  $s \approx 0$ .

**Setup:** Two different geometry models were used, namely, a standard S- $\alpha$  model, and an analytical model which patches circular and hyperbolic magnetic flux surface contours together to mock-up an X-point like singularity. It is noteworthy that, even though the local version of the turbulence model has been used here, both geometrical models allow for a self-consistent treatment of the MHD equilibrium that comes into play whenever the profiles of the dependent variables are evolved in time [2, 5]. The relevant quantities are depicted in Fig. 1. The nominal plasma parameter chosen are representative of a modern tokamak edge plasma,

$$\hat{\epsilon} = 18350, \quad \hat{\mu} = 5.0, \quad \hat{\beta} = 1, \quad C = 2.55, \quad \hat{s} = 1.0 \text{ (magnetic shear)}$$

$$\tau_i = T_i/T_e = 0, \quad L_{\perp} = L_T = L_n \quad \text{and} \quad \omega_B = 2L_{\perp}/R = 0.05$$

which correspond roughly to the physical quantities:  $T_0 = 70\text{eV}$ ,  $n_0 = 1.6 \times 10^{13}\text{cm}^{-3}$ ,  $M_i = 3670m_e$ ,  $R = 165\text{cm}$ ,  $a = 50\text{cm}$ ,  $L_{\perp} = 4.1\text{cm}$ ,  $B = 2.0\text{T}$  and  $q = 3.4$ . A scan in resistivity, which amounts to changing the values of  $T_0, n_0$  while keeping the remaining parameters fixed, was made within the set  $\nu \in \{1, 2, 5, 10, 20, 50, 100, 200\}$  with  $C = 2.55\nu$ . The grid count was  $32 \times 128 \times 16$  in  $\{x, y, s\}$  for all the cases with S- $\alpha$  geometry and with double number of nodes in the  $s$ -direction for the X-point geometry, to resolve the higher degree of structure in that case (see. Fig. 1). The necessary sub-grid dissipation was yield by using a perpendicular hyperviscosity

of 0.01 and parallel viscosity of 0.01 (0.005 for the X-point case).

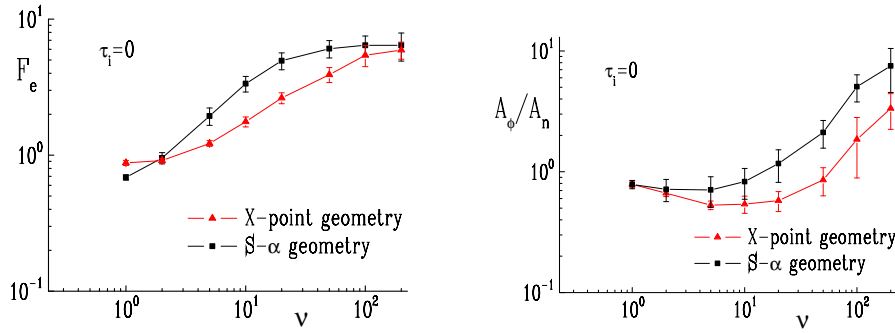


Figure 2: Volume averaged (left) electron particle flux and (right) amplitude ratio  $(\tilde{\phi}^2/2)/(\tilde{n}_e^2/2)$  (for  $k_y \neq 0$  only) averaged within the turbulent saturated phase,  $1000 \leq t/(L_\perp/c_s) \leq 3000$ , vs. resistivity.

**Results:** The two integral quantities shown in Fig. 2, namely, the electron particle flux and the ratio of the squared amplitudes of  $\tilde{\phi}$  and  $\tilde{n}_e$  are of particular relevance to assess the competition between drift wave and interchange physics. The plot on the right side shows the typical behaviour for the S- $\alpha$  case, namely, the energy contained in  $\tilde{\phi}$  and  $\tilde{n}_e$  is similar for moderate resistivity  $1 < \nu < 10$ , a typical signature for drift wave turbulence. For higher resistivities,  $\tilde{\phi}$  gets stronger as the resistive coupling to the density mediated by the parallel currents (nonadiabaticity) weakens ( $\tilde{J}_\parallel = C^{-1} \nabla_\parallel (\tilde{n}_e - \tilde{\phi})$ ), leaving only the interchange effects, via curvature, to transfer energy between them. This accounts for the increased transport (Fig. 2-left) as the phase shift between  $\tilde{n}_e$  and  $\tilde{\phi}$  increases towards the ideal interchange value  $\pi/2$  (diagnostic measured by not shown here), for which transport is maximal. The X-point case shows also a similar trend in transport based on similar grounds, but it further shows an overall lower transport level, which can be attributed to the enhancement effect on nonlinear breaking of vortical structures due to the sharp increase in the local shear [6] associated with the X-point (Fig. 1). Nevertheless, the picture gets more involved in this case, as also the variation of  $B^2$  amplitude along the field lines (Fig. 1) plays an important role by affecting the polarisation drift dynamics since a stronger vorticity is allowed ( $\tilde{\Omega} = \nabla_\perp^2 \tilde{\phi}/B^2$ ). One would then expect this to contribute also to an higher degree of coupling between  $\tilde{\phi}$  and  $\tilde{n}_e$ , mediated by the currents ( $\tilde{J}_\parallel$ ), based on the fact an higher vorticity yields higher nonlinear polarisation drift, which then leads to higher parallel currents available to balance it and maintain quasi-neutrality. The values for the squared amplitudes ratio (Fig. 2-right) for the X-point case support this picture. The curve starts to rise significantly only for  $\nu > 50$ , whereas this happens earlier ( $\nu > 20$ ) in the S- $\alpha$  case. Still to be investigated in detail is the role of the remaining geometrical quantities using control tests, by selected ones are reverted back to the S- $\alpha$  values to infer on their isolated effect.

More detailed assessment of the energy transfer paths between the background density gradient and the turbulence via drift wave and interchange processes is possible by diagnosing the

$E \times B$  energy theorem for each toroidal mode number  $l$ , given by

$$\sum_{i,k} \frac{1}{N_x N_y} 2\Re \left\{ \tilde{\phi}_l^* \left[ \left( \frac{\partial}{\partial t} (\tilde{n}_i - \tilde{n}_e) \right)_l = \underbrace{[\mathbf{v}_E \cdot \nabla (\tilde{n}_e - \tilde{n}_i)]_l}_{\text{polarisation drift}} - \underbrace{[\nabla_{\parallel} (\tilde{u}_{\parallel} - \tilde{v}_{\parallel})]_l}_{\text{nonadiabaticity}} + \underbrace{[K(\tilde{n}_e)]_l}_{\text{interch. forcing}} \right] \right\}$$

where the sums are over the all the  $N_x$  and  $N_y$  grid nodes in  $(x, s)$  directions, and the cold-ions approximation was used (vorticity is  $\tilde{\Omega} = \tilde{n}_e - \tilde{n}_i$ ). Fig. 3 shows the results. The left most plot

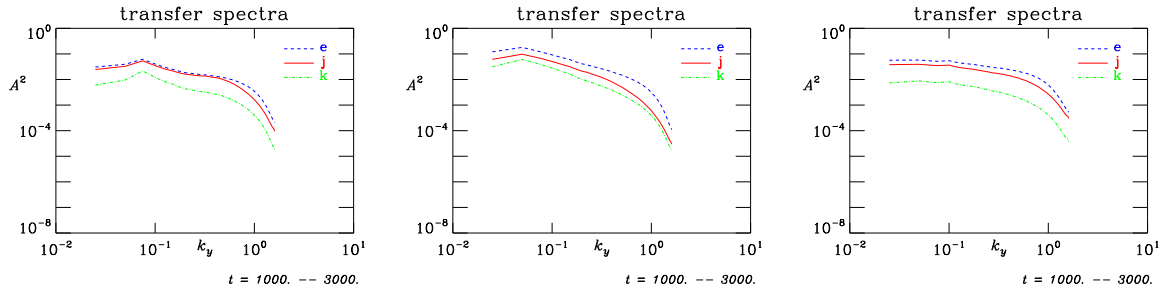


Figure 3:  $E \times B$  transfer spectra for S- $\alpha$  geometry (left)  $\nu = 5$ , (centre)  $\nu = 20$  and (right) X-point geometry and  $\nu = 20$ , all averaged over the interval  $1000 \leq t/(L_{\perp}/c_s) \leq 3000$ , for (e)  $\mathbf{v}_E \cdot \nabla \tilde{\Omega}$ ; (j)  $\nabla_{\parallel} \tilde{J}_{\parallel}$  and (k)  $K(\tilde{n}_e)$ . The modulus of each transfer term has been taken because one is not interested in the direction (direct or inverse) of the energy transfer, but rather on the total amount transferred.

( $\nu = 5$ ) shows a typical drift wave regime, where the nonlinear polarisation drift ( $\mathbf{v}_E \cdot \nabla \tilde{\Omega}$ ) is the largest term, followed closely by the nonadiabaticity ( $\nabla_{\parallel} \tilde{J}_{\parallel}$ ), indicating that the drift wave physics provide the main channel for energy transfer in this case. The interchange forcing term ( $K(\tilde{n}_e)$ ) is subdominant and can not account for the level of nonadiabaticity measured. As  $\nu$  increases, the picture starts to change and the interchange forcing becomes more important (centre plot). Then, also the spectra shifts to lower  $k_y$ 's as larger ballooning structures due to the interchange physics becoming more important. The last plot shows the  $\nu = 20$  case with X-point geometry, where one sees 1) the interchange forcing is less important than for corresponding S- $\alpha$  case (it is actually closer to the S- $\alpha$  case with  $\nu = 5$ ) and 2) that less energy content is available for the lower  $k_y$ 's, due to the local shear decorrelating effect. The main ideas presented are also supported by other mode structure diagnostics not shown here due to space constraints.

In sum, it has been shown that the X-point has a stabilising geometrical effect on turbulence, by limiting the size that the turbulent vortices can reach. This, together with the changes in the nonlinear polarisation drift, seems to have an effect of delaying the transition from drift wave into interchange turbulence. Extension of this work with the control test cases on the geometry and inclusion of warm-ions is foreseen.

## References

- [1] B. Scott *Phys. Plasmas* **12**, 062314 (2005)
- [2] T. Ribeiro, *30th EPS Conf. on Control. Fusion Plasma Phys.* ECA **31F**, P-4.055 (2007)
- [3] B. Scott *Phys. Plasmas* **12**, 102307 (2005)
- [4] B. Scott *Phys. Plasmas* **8**, 447 (2001)
- [5] B. Scott, *Contrib. Plasma Phys.* **46**, 714 (2006)
- [6] A. Kendl and B. Scott, *Phys. Rev. Lett.* **09**, 35006 (2003)